INFLUENCE OF STRAIN RATE FOR NOTCH- BEND STRENGTH ON DUCTILE CAST IRON

T. Ikeda[1,2], T. Umetani[1], N. Kai[1], N-A. Noda[2] and Y. Sano[2]

[1] HINODE, Ltd., Azaiwasaki, Miyaki-cho, Miyaki-gun, Saga, 849-0101 Japan
[2] Kyushu Institute of Technology, Sensui-cho, Tobata-ku, Kitakyushu, Fukuoka, 804-8550 Japan

Abstract: In this study, the notch-bend strength ($\sigma_{b,max}$) which is useful to structural design was considered for High Si Solid Solution Strengthened Ferritic Ductile Cast Iron. Then, the application of the high Si ductile cast iron to wide industrial fields was discussed at room temperature. Dynamic three-point bending tests were conducted on Charpy V-notch specimens in the range of stroke speed, $10^{-3}\sim10^{2}$ mm/s, at 22°C. Even though the absorbed energy of fracture process was in the lower shelf region, the notch-bend strength ($\sigma_{b,max}$) did not decrease with increasing the strain rate. These results indicate $\sigma_{b,max}$ is insensitive to the strain rate. Therefore, the authors think that the high Si ductile cast iron has wide industrial application potentiality at room temperature.

Keywords: high Si ductile cast iron, notch-bend strength, strain rate, temperature

1   INTORODUCTION

Conventional ferrite-pearlite type ductile cast irons are widely used for auto parts, mechanical parts and structural members. In recent years, High Si Solid Solution Strengthened Ferritic Ductile Cast Iron (high Si ductile cast iron) has been attracting attention as a new candidate for various mechanical and structural components [1-3]. This material has been already standardized in EN 1563 with the tensile strength in the range of 450~600MPa at the Si content in the range of 3.0~4.3% [4]. High Si ductile cast iron shows much smaller section thickness sensitivity because of higher silicon content than normal 2.0~2.7%Si. Furthermore, elongation and fatigue strength of this material are higher than that of a similar strength level of conventional ferrite-pearlite ductile cast iron [5]. Those advantages indicate wide industrial application potentiality of this material. On the contrary, high Si ductile cast iron shows a brittle fracture near room temperature in Charpy impact test, since the ductile-brittle transition temperature rises with the increase in Si content [6-8]. This is one of the reasons why the industrial application of high Si ductile cast iron is still very limited. However, it should be noted that Charpy absorbed energy has not been directly used as design strength. Therefore, the notch-bend strength ($\sigma_{b,max}$) was considered with varying the strain rate at room temperature. In this study, the dynamic three-point bending tests will be conducted controlling the stroke speed=$10^{-3}\sim10^{2}$ mm/s at 22°C for Charpy V-notch specimens. Then, the application of the high Si ductile cast iron to wide industrial fields is discussed at room temperature.

2   EXMENTAL PROCEDURES

2.1 Material

Table 1 shows chemical composition of test specimens. Type-B Y-shaped blocks (JIS-G 5502) [9] shown in Fig.1 are cast in sand molds. All tests specimens are taken from the as cast specimens of the highlighted sections in gray whose dimensions are 40×25×250 mm in Fig.1. Figure 2 shows typical microstructures of test specimens. As shown in Fig.2, test specimen has fully ferritic matrix. Table 2 shows the tensile property of test specimen based on JIS No.4 test piece whose diameter=14mm and gage length=50mm [10]. The test procedure meets JIS-Z 2241 standard.

Table 1 Chemical compositions of as cast specimens (mass %)

C	Si	Mn	P	S	Cu	Mg
3.20	3.72	0.32	0.022	0.008	0.02	0.038

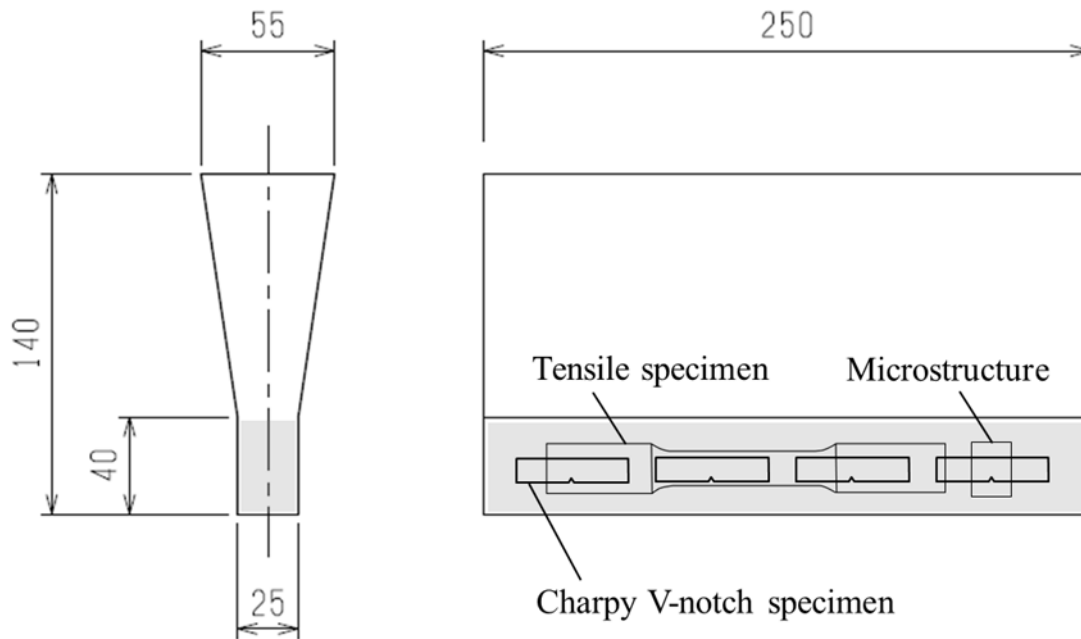**Fig. 1** Schematic view of Y-sharped block
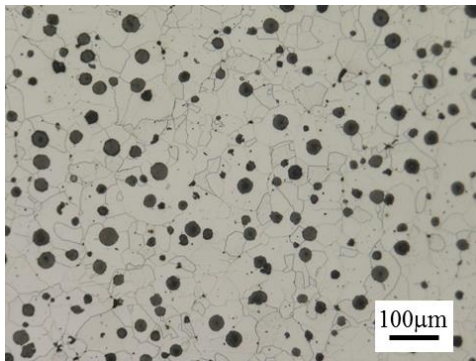
Fig.2 Microstructures of as cast specimen

Table 2 Tensile properties of test specimen

σ_B (MPa)	525
$\sigma_{0.2}$ (MPa)	401
ε_B (%)	21

σ_B:Tensile strength

$\sigma_{0.2}$:0.2% proof stress,

ε_B:Fracture strain

2.2 Charpy impact test

Figure 3 shows Charpy V-notch specimen dimensions. All the tests use this shape of specimen. The impact test is performed using a Charpy impact machine with 300J maximum energy capacity. The impact speed is 5.18×10^3 mm/s. The total absorbed energy in the fracture process E_c is determined by measuring the decrease in motion of the pendulum arm [11]. The ductile fracture surface ratio f_D is determined macroscopically from microscope photograph for showing the fracture morphology. The procedures meet JIS-Z 2242 standard [11].

2.3 Dynamic three-point bending test

To control loading speed, three-point bending test is conducted using V-notch specimen (Fig.3). This test is carried out in the range of stroke speed, $v = 10^{-3} \sim 10^2$ mm/s, at 22°C by using electrohydraulic servo testing machine. The bending jig whose span length $L_s = 40$mm has the same shape and size as the Charpy impact testing machine. The strain rate $\dot{\varepsilon}$ is calculated by using equation (1) [12-15], where h = test specimen width, Q = 1.94 [12-15], v = stroke speed, L_s = span length.

$$\dot{\varepsilon} = 6hvQ / L_s^2 \tag{1}$$

The total absorbed energy E_t in the fracture process is also obtained from area under the load-deflection curve of the three-point bending test. The fractographic analysis is performed by optical observations and scanning electron microscopy (SEM). The ductile fracture surface ratio f_D is determined macroscopically from microscope photograph.
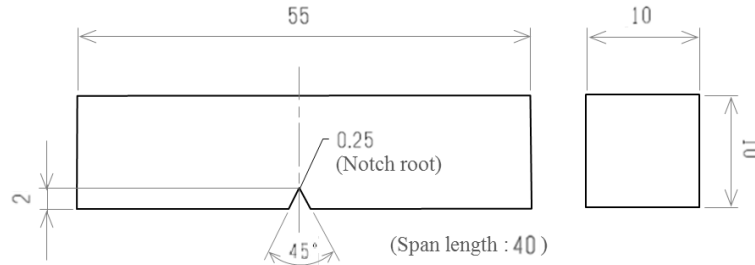

Fig. 3 V-notch specimen dimensions (JIS-Z 2242)

3   RESULTS AND DISCUSSION

3.1   Charpy transition curve

Figure 4 shows the results of V-notch Charpy impact test. In Fig.4(a), the absorbed energy E_c starts dropping at the critical temperature for upper shelf region of 80°C as indicated by the black arrow. In Fig.4(b), f_D starts dropping at the same critical temperature of E_c. Brittle fracture surface appears below this critical temperature. In Fig.4 (a), (b), a good coincidence can be seen for the transition of E_c and f_D. This means that the reduction of E_c is caused by ductile-brittle fracture surface transition. In Fig.4(a), lower shelf region is recognized and ductile fracture surface completely disappears below 20°C, Fig.4(b).
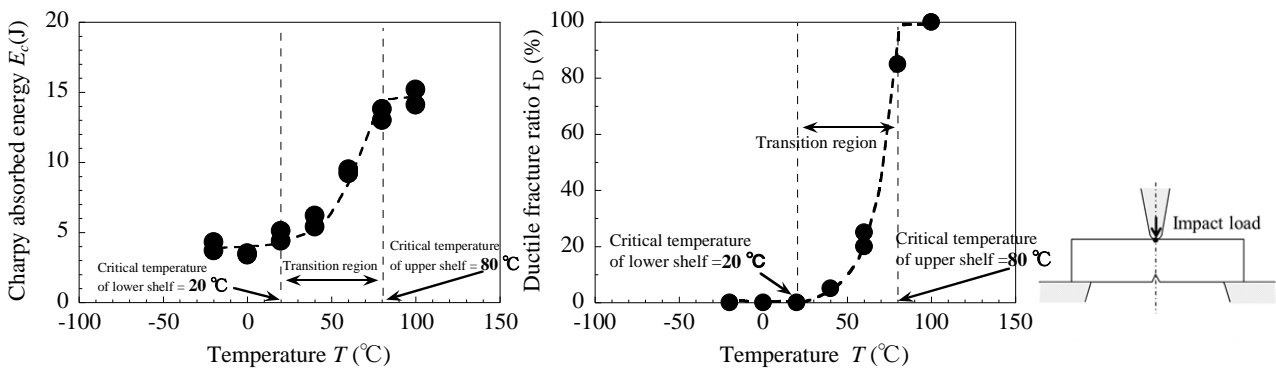

(a) Transition curves of absorbed energy   (b) Transition curve of ductile fracture ratio

Fig. 4 Result of Charpy impact test

3.2   Absorbed energy depending on strain rate

Figure 5 shows the effects of the strain rate $\dot{\varepsilon}$ on (a) the absorbed energy E_t and (b) the f_D of the three-point bending test at 22°C. In Fig. 5(a), the upper shelf region is being recognized even at 22°C, room temperature. In Fig.5, the upper shelf energy is obtained because these $\dot{\varepsilon}$ are more than 10^3 times lower than $\dot{\varepsilon}$ of Charpy impact test. In Fig.5(a), the absorbed energy starts dropping at $\dot{\varepsilon}$ of $2.5 \times 10^{-1} \text{s}^{-1}$ as indicated by the black arrow. Brittle fracture surface appears above this critical $\dot{\varepsilon}$. Similar to the results of Charpy impact test a good coincidence can be seen for the transition of E_t and f_D. It may be concluded that the reduction of E_t is caused by ductile-brittle fracture surface transition by increasing $\dot{\varepsilon}$.
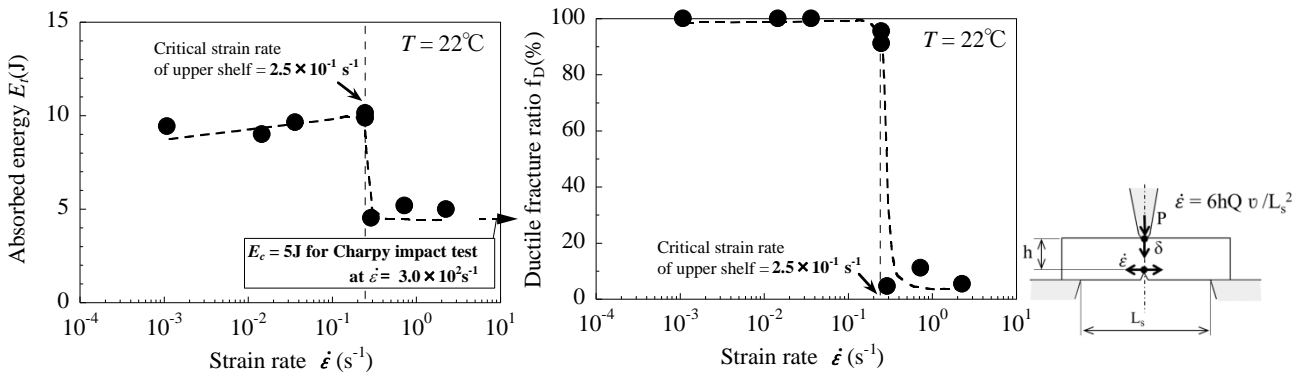
(a) Effect of strain rate on absorbed energy   (b) Effect of strain rate on ductile fracture ratio

Fig. 5 Result of the three-point bending test at 22°C

3.3   Notch-bend strength insensitive to strain rate

Absorbed energy has not been directly used as design strength. Therefore, the strength was considered with varying the strain rate at 22°C, room temperature. Figure 6 shows a load-displacement curve on the three-point bending test under different $\dot{\varepsilon}$ at 22°C. From Fig.6, it is seen that the maximum displacement δ_{max} decreases with increasing $\dot{\varepsilon}$. This is why E_t decreases with increasing $\dot{\varepsilon}$ in Fig.5(a). On the contrary, in Fig.6, it should be noted that the maximum load P_{max} slightly increases with increasing $\dot{\varepsilon}$. Figure 7 shows the relationship between the notch-bend strength $\sigma_{b,max}$ and $\dot{\varepsilon}$ for the three-point bending test at 22°C. The notch-bend strength $\sigma_{b,max}$ was calculated by equation (2) [16,17], where P_{max} = maximum load, Ls = span length, b = test specimen thickness, h = test specimen width.

$$\sigma_{b,max} = 3P_{max}Ls \ / \ 2bh^2 \tag{2}$$

For comparison, the relationship between E_t and $\dot{\varepsilon}$ shown in Fig.5(a) is also put in Fig.7. In Fig.7, it should be noted that even though E_t is in the lower shelf region, the notch-bend strength, that is $\sigma_{b,max}$, does not decrease insensitive to $\dot{\varepsilon}$. The authors think that high Si ductile cast iron has a wide industrial application potentiality because the notch-bend strength insensitiveness to $\dot{\varepsilon}$ although the absorbed energy is sensitive.
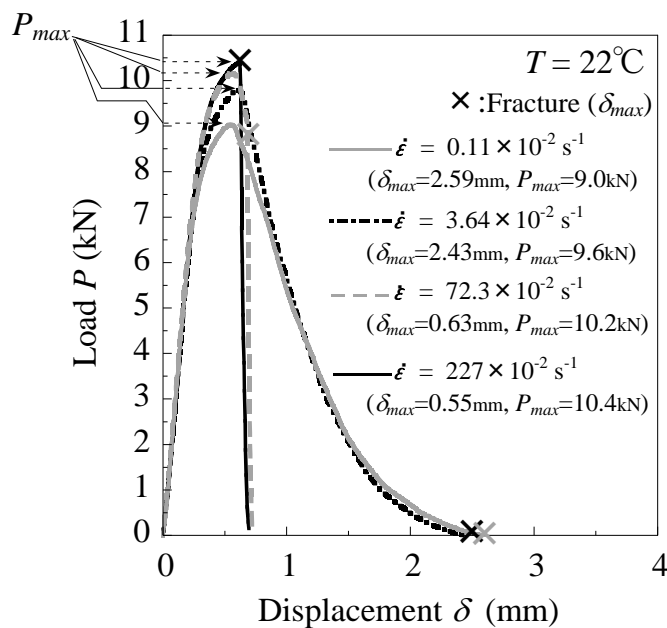

Fig. 6 Variation of load-displacement curves of the three-point bending test with strain rate at 22°C
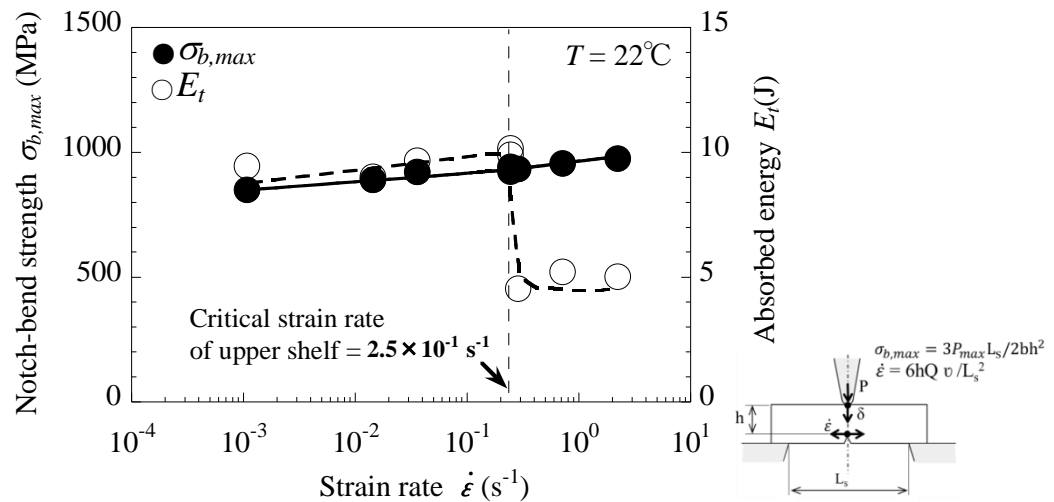
Fig. 7 Effect of strain rate on the notch-bend strength of the three-point bending test at 22°C

4   CONCLUDION

In this study, the notch-bend strength was considered for high Si ductile cast iron. This material has attracted a lot of attention recently because of smaller section thickness sensitivity and higher fatigue strength. Dynamic three-point bending test were conducted in the range of stroke speed, $10^{-3} \sim 10^2$ mm/s, at 22°C. The conclusions can be made the following way.

(1) The absorbed energy E_t decrease with increasing $\dot{\varepsilon}$. The reduction of E_t is caused by ductile-brittle fracture surface transition by increasing $\dot{\varepsilon}$.

(2) Even though the absorbed energy E_t is in the lower shelf region, $\sigma_{b,max}$ does not decrease with increasing $\dot{\varepsilon}$ in the range of $\dot{\varepsilon}$, $1.1 \times 10^{-3} \sim 2.3 \times 10^0 \mathrm{s}^{-1}$, at 22°C. Notch-bend strength $\sigma_{b,max}$ is insensitive to strain rate $\dot{\varepsilon}$ at 22°C, room temperature.

Therefore, the authors think that $\sigma_{b,max}$ is more useful than absorbed energy for structural design. The high Si ductile cast iron has wide industrial application potentiality at room temperature.

5   REFERENCES

[1] R.Larker, Solution strengthened ferritic ductile iron ISO 1083/JS/500-10 provides superior consistent properties in hydraulic rotators, China Foundry, 6, 343-351, 2009.

[2] R.Larker, Paradigm shift in revised 1563(GJS) enables improved properties and production economy in both as-cast and austempered (ADI) states, Proc. NEWCAST Forum, Bundesverband der Deutschen Gießerei Industrie, Düsseldorf, 29-34, 2011.

[3] H.Löblich, W.Stets, Die Einführung von mischkristallverfestigtem Gusseisen mit Kugei-graphit in die Industrie-eine Erfolgsstory, Proc. Deutscher Gießereitag 2013 und 5. NEWCAST Forum, Verein Deutscher Giessereifachleute, Fellbach, 14-17, 2013.

[4] EN 1563, Founding-Spheroidal graphite cast irons, 2011.

[5] T.Umetani, T.Ikeda, N.Sura, K.Ashizuka, T.Nemoto, H.Takada, K.Ogi: Tensile Strength, Fatigue Strength, and Impact Strength of Solution Strengthened High Silicon Ferritic Ductile Cast Iron, J.JFS., 86, 36-42, 2014.

[6] T.Okumoto, T.Aizawa, Effect of Silicon Phosphorus and Pearlite on the Impact Transition Curves of Spheroidal Graphite Cast Irons, Imono, 35, 670-677, 1963.

[7] K.Nagai, K.Kishitake, T.Owadano, The Effect of Silicon Content on the Impact Fracture Characteristics of Ferritic Spheroidal Graphite Cast Irons, Imono, 58, 350-355, 1986.

[8] H.Nagayoshi, H.Yasuda, K.Imanishi, Effects of Silicon Content on Impact Properties of Spheroidal Graphite Cast Iron, J.JFS., 68, 506-511, 1996.

[9] JIS-G5502, Spheroidal graphite iron castings, 2001.

[10] JIS-Z2241, Metallic materials-Tensile test-ing-Method of test at room temperature, 2011.

[11] JIS-Z2242, Method for Charpy pendulum impact test of metallic materials, 2005.

[12] R.Sandstrom, Y.Bergstrom, Rerationship between Charpy V transition temperature in mild steel and various material parameters, Met. Sci., 18, 177-186, 1984.

[13] H.Yamamoto, T.Kobayashi, H.Fujita, Strain Rate Dependency of Ductile-Brittle Transition Behavior in Ductile Cast Iron, J.JFS, 72, 107-112, 2000.

[14] N.Sugiura, T.Kobayashi, I.Yamamoto, S.Nishido, K.Hayashi, Comparision of tensile and 3-point bend properties under impact loading in an AC4CH-T6 aluminum casting alloy, J. Jpn. Inst. Light Met.,45, 638-642 1995.

[15] K.Matsugi, G.Bando, G.Sasaki,O. Yanagisawa, Fracture Propaties at Elevated Temperatures of Ferritic Ductile Cast Irons, J.JFS., 79, 229-234, 2007.

[16] T. Kobayashi, H.Matsubara, Y.Ueda, Fracture Characteristics Obtained from Instrumented Impact Test of A533B Steel for Reactor Pressure Vessel, Tetsu-to-Hagané, 69, 1183-1189, 1983.

[17] S. Nunomura, M. Nakashiro, Fracture Characteristics Evaluation by Charpy Impact Bending Test, Tetsu-to-Hagané, 64, 860-868,1978.